EXPERIMENTAL MEASUREMENTS, CFD SIMULATIONS AND MODEL FOR A HELIUM RELEASE IN A TWO VENTS ENCLOSURE

G. Bernard-Michel[1], E. Saikali[1], D. Houssin[2]

[1] *D.E.N, D.A.N.S, S.T.M.F, L.E.I.F.T, Bât. 460, CEA Saclay, Gif-Sur-Yvette, France, e-mail : gilles.bernard-michel@cea.fr and elie.saikali@cea.fr*

[2] *Air Liquide - Centre de Recherche Claude-Delorme, chemin de la Porte des Loges, Les loges-en-Josas 78354, France, e-mail : deborah.houssin@airliquide.com*

ABSTRACT

The present work proposes improvments on a model developped by Linden to predict the concentration distribution in a 2 vented cavities. Recent developments on non constant entrainment coefficient from Carazzo *et al* as well as a non constant pressure distribution at the vents - the vents being vertical - are included in the Linden approach. This model is compared with experimental results from a parametric study on the influence of the height of the release source on the helium dispersion regimes inside a naturally ventilated 2 vents enclosure. The varying parameters of the study were mainly the height of the release, the releasing flow rate and the geometry of the vents. At last, Large Eddy Similations of the flow and Particle Image Velocimetry measurements performed on a small 2 vented cavity are presented. The objective is to have a better understanding of the flow structure which is at the origin of the 2 layers concentration distribution described by Linden.

I. CONTEXT

Experimental and numerical studies on the dispersion of buoyant jet in confined but naturally ventilated environment are carried out for risk assessment of hydrogen release in confined volume. Recently experimental measurements of helium concentration dispersion were performed by several authors [1–4] in large scale enclosure equipped with two ventilation openings. Some works are also characterizing the flow in such cavities through L.E.S numerical simulations [5]. This work aims at validating an improved model for the natural ventilation through two openings in enclosures of smaller volumes, with a specific geometry close to existing hydrogen energy applications in case of accidental release. For safety reasons, experiments are performed with helium as releasing source, as it is proved to be a good substitution to hydrogen [6]. Based on this information, several points could be improved like analytical models for risk assessment, safety devices (type and performance) for the hydrogen energy systems and design recommendations for future applications. The first section of this paper presents briefly the context of this work. In the second section, engineering simple approaches commonly used for maximal concentration assessment at the steady state. In the third section the experimental setup is described. Then in the fourth part, results are presented and discussed. In the fith part we developped an improved model based on Linden work [7, 8] on the concentration distribution two-layers strucutre and also based on kaminski [2] improved model for the entrainment coefficient. At last in the sixth part, we illustrate the flow behaviour based on

L.E.S numerical simulations [5] as well as PIV measurements performed on small 2 vented enclosure (3/8 of a litre) before concluding.

II. EXISTING MODELING APPROACH

The enclosure is naturally ventilated thanks to two vertical vents localized one near the floor, the other near the ceiling as shown in Figure 1.

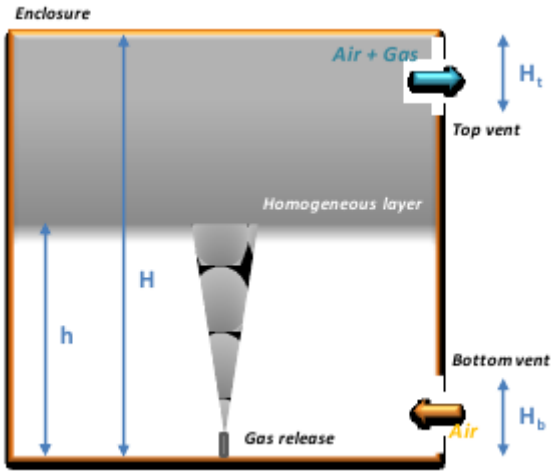

FIG. 1: Scheme of the dispersion phenomenon considered in a naturally ventilated enclosure with two openings localized at different altitudes.

Baines and Turner model [9] was extended by Linden [7, 8] to consider an enclosure connected by upper and lower vents to external environment. Replaced in the context of a buoyant gaz flow, Linden showed that a simple stratification develops consisting in two layers separated by a horizontal interface. The lower layer has a uniform concentration and contains only pure air whereas the upper layer is also at a uniform concentration but with a helium/air mixture. The presence of the upper buoyant layer creates a pressure difference across the vents, which in turn drives a draining flow. A steady state is reached when this draining flow is balanced by the convective plume flow. Linden proposes a methodology to calculate, at steady-state, the concentration of the homogeneous upper layer and the height of the interface.

$$X_f = \frac{1}{C}\left(\frac{Q_0^2 h^{-5}}{g_0'}\right)^{1/3}, \tag{1}$$

where X_f is the volume fraction of releasing gas, Q_0 is the releasing gas flow rate, h is the height of the interface, g_0' is the reduced gravity, C is a constant given by the plume theory of Morton et al. [10]:

$$C = \frac{6}{5}\alpha \left(\frac{9}{10}\alpha\right)^{1/3} \pi^{1/3}, \tag{2}$$

where α is the entrainment coefficient (from 0.05 to 0.15 for a pure plume). The height of the interface, h, is given by the following expressions:

$$\frac{S^*}{H^2} = C^{3/2} \left(\frac{(h/H)^5}{1-h/H}\right)^{1/2}, \tag{3}$$

$$S^* = \frac{\sqrt{C_t} S_t S_b}{\left(\frac{1}{2}\left(\frac{C_t}{C_b} S_t^2 + S_b^2\right)\right)^{1/2}}, \tag{4}$$

where S^* is the effective vent area, H the difference height between top and bottom vents, C_t the top vent discharge coefficient, C_b the bottom vent discharge coefficient, S_t the top opening area, S_b the bottom opening area.

This approach, commonly used as engineering tool for build-up assessment, does not allow the height of release to be considered; i.e. release is considered at the floor. As we will see later, we advise to consider the parameter H as the altitude separating the upper edge of the top vent from the injection's height. In this case, h has to be considered as the interface's height starting from the injection's height as a reference point. Nevertheless we will propose further improvement to the model since it does not take into account the vertical orientation of the vents, neither varying entrainment coefficient along the jet height.

III. EXPERIMENTAL SETUP

A. Test bench description

The Plexiglas enclosure is a rectangle parallelepiped with a square horizontal base of an internal volume of 2 $\mathbf{m}^3$ (see Figure 2). The internal size of the enclosure are a 98 cm length and width, for a 2.10 m height. The enclosure has two openings for natural ventilation study: one at the top, and one at the bottom, localized on the same vertical face as shown in Figure 1(B). The bottom opening has a fixed size of h19 x w98 cm, whereas the height of the top opening can be changed: 19, 8.5 and 4.5 cm (the width remaining constant: 98 cm). It should be noted that due to the metal frame of the inclosure, the top vent is located at 2.06 m heigh, that is 4 cm below the internal ceiling of the enclosure. The bottom vent is located 4 cm above the internal floor of the enclosure for the same reason.

The helium injection source is a PVC circular tube of 27.2 mm of internal diameter, centered in the horizontal square section, directed upward. The pipe is long enough so that a Poiseuille flow

is fully developed at the injection. The outlet of the injection tube is localized at several altitudes from the bottom: from 27 cm to 197 cm. The range of tested flow rates is 1 NL.min^{-1} up to 210 NL.min^{-1} . Injections were performed with two mass flow controllers chosen accordingly to the desired flow rate. One regulator has a 20 NL.min^{-1} full scale and the other has a 350 NL.min^{-1} full scale. The error on the mass flow rate for the 20 NL.min^{-1} controller is 0.1% of full scale plus 0.5% of the set point. For the 350 NL.min^{-1} controller, the error on the mass flow rate is 0.2% of full scale plus 0.7% of the set point. Taken into account the release diameter of 27.2 mm, the volume Richardson range studied in this work is from $8.01 \cdot 10^4$ down to 1.82 for respectively 1 and 210 NL.min^{-1} .

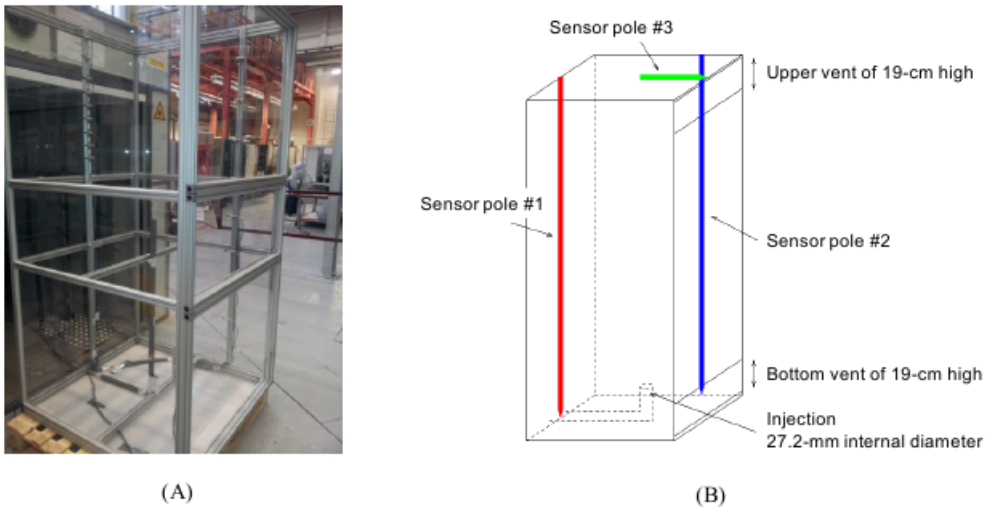

FIG. 2: Grand-Gamelan 2 $\mathbf{m}^3$ build-up enclosure. (A) Picture of the enclosure, (B) location of the sensors in the enclosure.

B. Measurement devices and data treatment

Based on the measurement of the thermal conductivity of the ambient gas, twenty one minicatharometers Xen-TCG3880 from Xensor Integration, are used to determine the volume fraction of the helium in the enclosure. Minicatharometers were calibrated before the experimental campaign. The absolute accuracy of the minicatharometers was assessed to be around 0.1% of helium volume fraction. Sensors can measure helium fraction fluctuations down to 0.05%. The reactivity of these sensors is assessed to be around 1 s.

Data treatment was automated: the time to reach steady state, the helium volume fraction mean and the corresponding standard deviation are calculated (Figure 3).

Pt-100 Platinum probes are integrated inside each helium sensor for temperature measurement inside the enclosure during experiments. The calibration of the platinum probes temperature gives an absolute accuracy of 0.5°C on temperature information. They can measure temperature fluctuations down to 0.1°C. Sensors are located on three sensor poles: two vertical poles, and one horizontal pole near the ceiling of the enclosure, as shown in Figure 2 (B). According to the studied

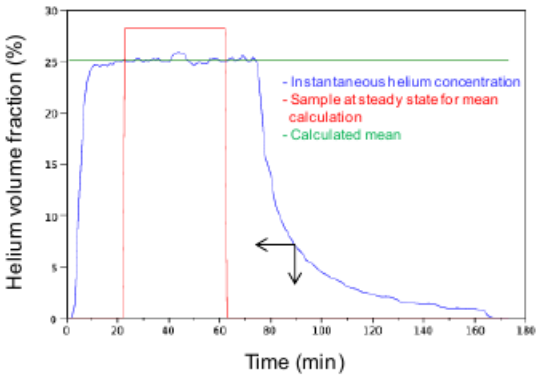

FIG. 3: Data treatment for steady state determination and corresponding measured helium volume fraction.

configurations, sensors location can change in order to optimize information on helium distribution in the enclosure (see Figure 4).

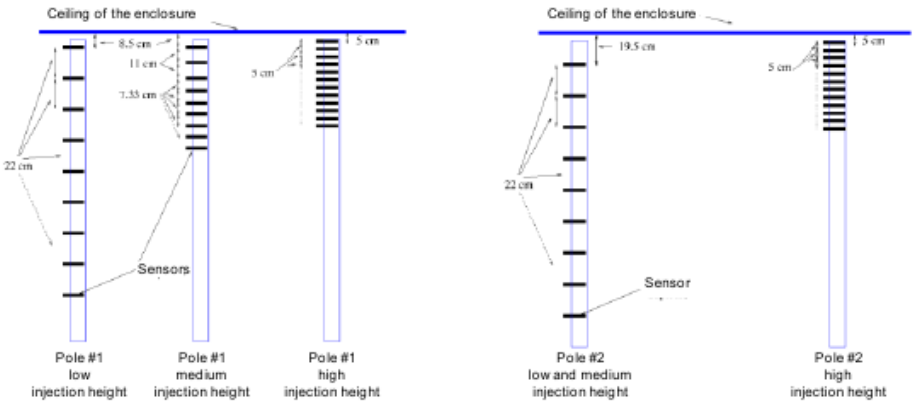

FIG. 4: Location of minicatharometers on sensor poles 1 and 2 according to the height of the injection.

C. 2 m^3 enclosure experimental configurations

Helium is injected at six heights: 27, 107, 138, 158, 168 and 197 cm from the bottom of the enclosure - oriented vertically upwards - through a circular nozzle of 27.2 mm internal diameter centered in the horizontal section of the enclosure. The releasing flow rate is injected in the enclosure when the targeted value is reached and correctly regulated by the mass controller. At this time helium concentrations measured by the minicatharometers as a function of the time and of the height are recorded each 5 s. The injection is stopped 5 to 10 minutes after reaching the steady state; i.e. when helium concentrations are steady with time. During gas injection, the stability of the temperature inside the enclosure is checked. The summary of the studied configurations is given in Table I. It has to be noticed that one configuration has a top vent located at a 1.45 m height

instead of 2.06 m. This is to confirm the non influence of the enclosure height on the maximum concentration, which is discussed later in the document.

bench serie	injection height	vent type	flowrates (NL/min)
1	27	1	1 5 10 15 20 35 70 105 140 210
2	107	1	1 5 10 20 35 70 105 140 210
3	197	1	1 3 5 10 20 35 70 105 140 210
4	197	2	1 5 35 210
5	197	3	1 5 20 210
6	188	1	1 210
7	188	2	1 210
8	188	3	1 20
9	178	3	1 20
10	168	3	1 5 10 20 35 70 210
11	168	2	1 5 10 20 35 70 140 210
12	168	1	1 5 10 20 35 70 140 210
13	158	1	1 3 5 10 20 35 70 140 210
14	158	3	1 3 5 10 20 35 70 140 210
15	158	2	1 5 20 70
16	138	1	1 3 5 10 20 35 70 140 210
17	138	1	1 10 210
18	67	1	1 5 10 20 35 70 105 140 210 350 700
19	128*	1	5 35 105 210

TABLE I: Studied configurations. vent type 1: 19cm x 98cm, type 2: 8.5cm x 98 cm and type 3: 4.5cm x 98 cm. The case 128* is particular. The top vent is located at a 145 cm height and the injection is in reality located at 67 cm height. The distance between the injection and the top vent is the same as if the injection would be at 128 cm and the top vent at an unchanged position of 206cm. It will be shown that indeed only the separating distance between injection and the top vent does matter hence the specific design for this bench number 19.

D. 3/8 $\mathbf{m^3}$ experimental configuration

We also consider a smaller enclosure, in order to perform both PIV measurements and CFD Direct Numerical and Large Eddy Simulations (DNS/LES). Here, we inject pure helium through a cylindrical pipe with a unique constant volumetric flow-rate $Q = 5$ Nl/min into a two vented parallelepiped enclosure filled initially with air at rest. All the physical properties of the light helium gas are referred to with the $_{in}$ subscript (meaning "injected"), while the subscript $_{am}$ is used to denote the ambient air. The pipe used for the injection is of diameter $d = 10^{-2}$ m and long enough to assure that a well developed Poiseuille flow is attained. The internal dimensions of the cavity are $W \times L \times H = 4.9{\times}5{\times}14.9 \times 10^{-6}$ m^3. We note that the height of the configuration H was selected so as to obtain a transitional flow regime from laminar to turbulent, predicted to occur at $H/d > 5$ [11]. The two vents are considered to be identical with a surface area $5{\times}2.9{\times}10^{-4}$ m^2 and both located on the right vertical wall. Plexi-glass of thickness 5×10^{-3} m is used for the solid wall boundaries. A schematic representation of the experimental set-up is shown in figure 5.

Velocities are mesured in the $x0z$ plan, Fig. 5, which is cutting the enclosure perpendicularly to the vents and containing the injection axis. A laser sheet of less than 1mm thickness is enlightning

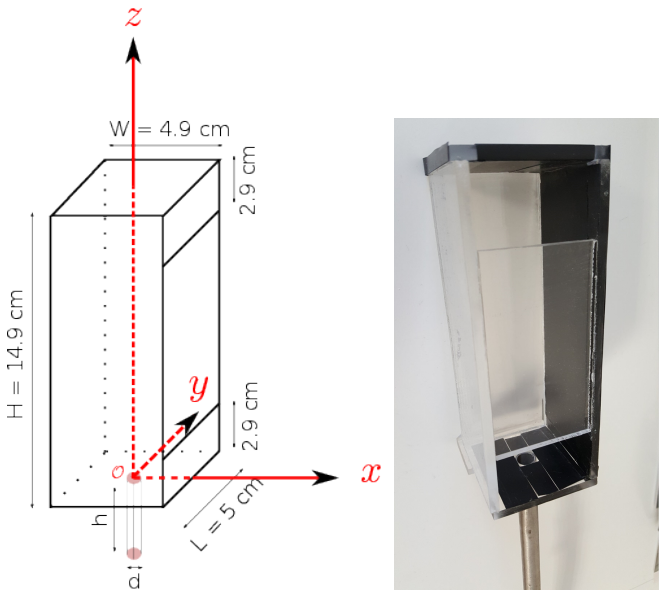

FIG. 5: Experimental set-up

Fluid	**Density** [kg.m^{-3}]	**Dynamic viscosity** [$\times 10^{-5}$ kg.m^{-1}.s^{-1}]	**Molar mass** [$\times 10^{-2}$kg.mol^{-1}]
Injected	$\rho_{in} = 0.16148$	$\mu_{in} = 1.918$	$M_{in} = 0.4003$
Ambient	$\rho_{am} = 1.16864$	$\mu_{am} = 1.792$	$M_{am} = 2.897$

TABLE II: Physical properties of the working fluids

that plan. Particles (smokes) are injected in the room, and oil dropplets are mixed with helium in the injecting tube with a specific device from DANTEC. All the particles are about 1 μm of diameter and follow the flow without any drift at the considered flow rates.

The laser light source is either a two cavities pulsed Yag (8 ns flash of 200 mJ) or a continuous Yag laser of 5 Watts. The pulsed laser (10 Hz) in used in association with a 8 Mpx PIV camera, whereas the continuous laser is used with a 1Mpx fast camera (2Khz). With the fast camera we perform measurement at the injection and also near the bottom vent. With the PIV camera, we cover the full enclosure but with slow frequency acquisitions of 1 Hz (to perform time average statistics). But every acquisition is made of two pictures separated by a small time interval (250 μs).

We calculate the velocity field using the free software GPIV delivered on ubuntu linux distributions. We use 16 x 16 px subframes with a 8 px shift and an predictor/corrector algorithm with distorded images capability. Basically, an estimate of the velocity is made, then subframed are moved and distorded according to that first prediction. A new velocity field is calculated and an iterative process is engaged until converged to a certain accuracy. Considering the quality of the pictures, we expect an absolute accuracy of 4% (checked on similar synthetical images) and a confidence of 95% on the data.

It as to be noticed that the accuracy is absolute, meaning that with an injection velocity of around 2 m/s, we expect a 0.08 m/s accuracy for the velocities. This is a problem at the bottom vent where velocities are around 0.3 m/s. That leads to a relative accuracy of roughly 25%. So we adopted 2 strategies to calculate the velocity fiekd: for the full field (pulsed yag laser), we calculate the velocity field on 2 successive images with the above mensionned absolute accuracy. It will provide a good description of the fastest regions of the flow. On the other hand, with the fast camera, we have the possibility to calculate the PIV correlation on 2 successive images, or between the first and the n^{th} following picture. Without getting into the details, this allows to calculate with less than 4% of error every desired range of the velocity. We used one image every 5 acquisition to evaluate the velocity field at the bottom vent, and between 2 successive acquisition for the full camera field. With this technique, the velocity relative error at the bottom vent is less than 4%.

The second source of error is the statistical error made when calculating the time-averaged quantities. With both techniques (fast camera and PIV camera), we manage to obtain 400 uncorrelated velocity fields per experiment. The statistical error for the averages is then 5 % of the measured standard deviation of the quantity. Therefore the statistical error never exceeds 2.5 % of the average quantity. In fact it is the PIV measurement which is the limiting factor in term of accuracy.

IV. EXERIMENTAL RESULTS

In this section we present the experimental results. First, we show that in most configurations we observe the same flow structure as Linden, that is: a 2 homogeneous layer structure of the concentration distribution. **The distance separating the upper vent from the injection is the main parameter controling the concentration distribution**. The height of the enclosure itself has no effect on the maximum concentration, but only on the time it takes to reach the steady state.

A. Three regimes for concentration distribution

We illustrate those three regimes with experiments achieved for two identical openings of 19 cm high and 98 cm width each. Figure 6 focuses on results for the extreme flow rates: 1 and 210 $NL.min^{-1}$ of helium relased at the lowest altitude of 27 cm. Independently of the helium fraction values, Figure 6 shows two different distribution profiles. For 1 $NL.min^{-1}$ the dispersion regime is stratified with an increase of the helium concentration with the altitude in the enclosure. While a bi-layer regime characterized by a homogeneous upper layer (concentration and thickness) is observed for 210 $NL.min^{-1}$, as the displacement ventilation described by Linden et al. [7, 8]. The bi-layer regime appears for flow rates higher than 10 $NL.min^{-1}$. For lower flow rates the dispersion regime is stratified: there is no homogeneous upper layer. Figure 7 shows the structure of helium distribution for a release located at 188cm from the bottom of the cavity.

We don't observe the displacement regime described by Linden but an impinging jet's concentration profile.

we can observe on the three precedent figures that the concentrations are the same on both sensors,

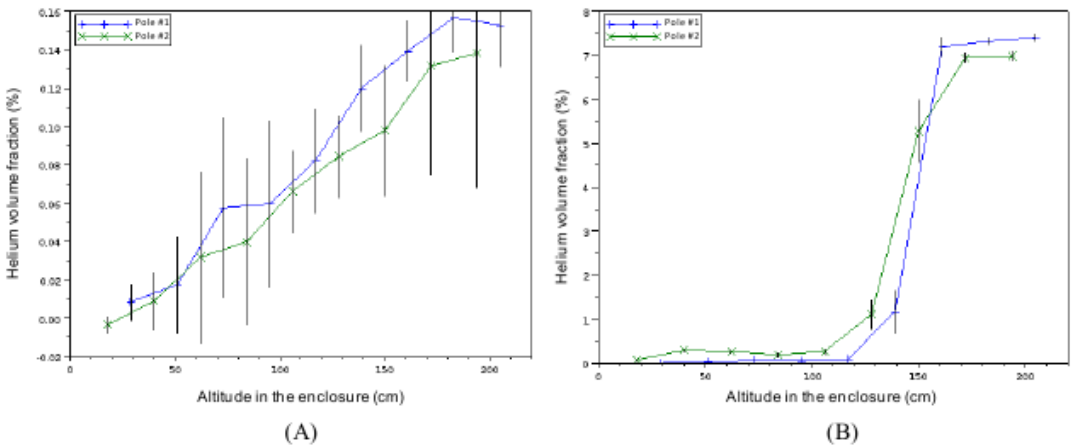

FIG. 6: Helium volume fraction as a function of the altitude in the enclosure and at steady state for 1 NL.min^{-1} (A) and 210 NL.min^{-1} (B) injected at 27 cm, with two vents of h19 x w98 cm each (vertical solid line: standard deviation).

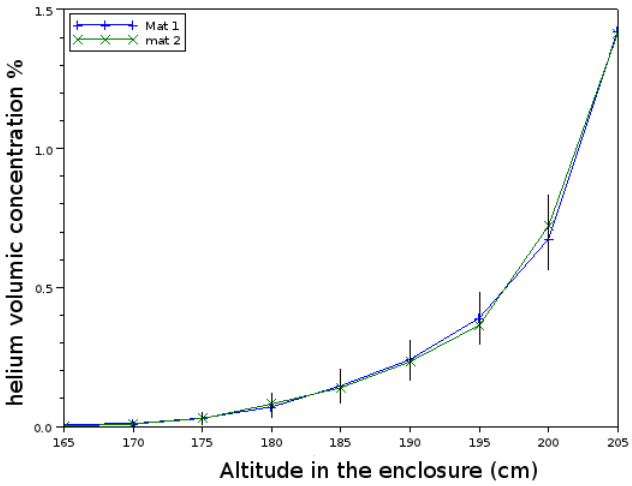

FIG. 7: Helium volume fraction as a function of the altitude in the enclosure and at steady state for 1 NL.min^{-1} injected at 188 cm, with two vents of h19 x w98 cm each (vertical solid line: standard deviation).

indicating that the concentration distribution is only dependant on the altitude z.

B. Summary for the existance of the displacement regime

We have summed up all the experimental results and classified them on a 2D plot (Figure 8) depending on the existence of a stratified layer, an impinging jet or a displacement regime with a

bi-layer structure of the concentration distribution.

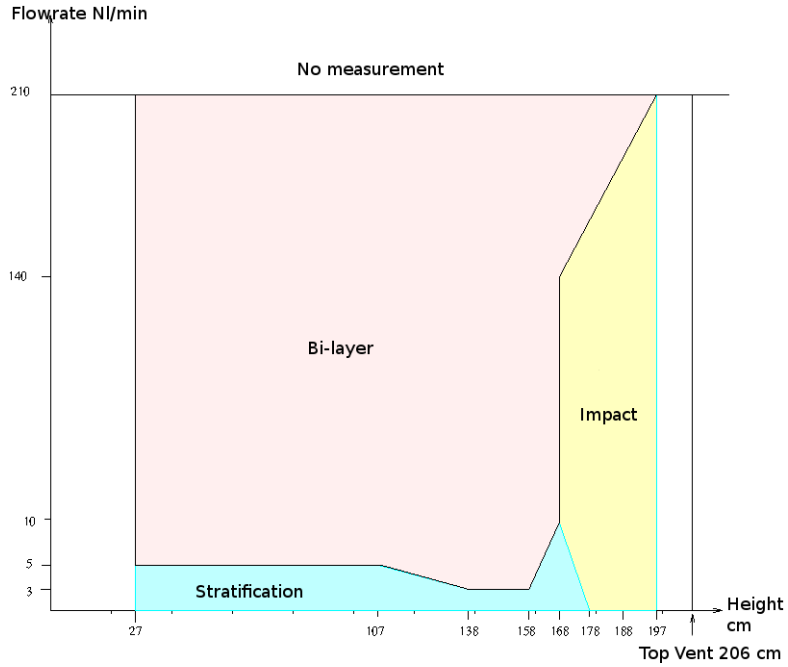

FIG. 8: Type of concentration distribution depending on the flow rate and the injection altitude.

We observe the displacement regime for the majority of the cases. For a distance between the injection and the top vent below approximately 40 cm, we don't observe it whatever the flow rate is. For larger distances, we observe the bilayer structure whenever the flow rate is above 10 NL.min^{-1} . Below that value, we observe a stratification of the helium concentration.

C. The distance between injection and top vent is the parameter of importance

In the following section, we will detail a modified Linden model to take into account a varying height of injection, vertical vents and a varying entrainment coefficient. We will see that the helium concentration in the upper layer depends on the flow rate and on the distance separating the top vent and the injection. We illustrate this in Figure 9 left, where we compare the expected analytical solution for an injection at an altitude of 128 cm with a top vent at 206 cm and the experimental concentration distribution for an injection at 67 cm and a top vent at 145 cm. The distance separating the vent and injection is the same for both scenarii and the obtained concentration profiles are similar.

We also notice, Fig. 9 right, that for the second case where injection is the same at a 67 cm hightbut with a top vent located at a 206 cm height, the maximum concentration for a flow rate of 210 NL.min^{-1} is approximately around 10 to 11%. With a top vent located at a 145 cm height (left figure), the concentration is approximately 17%. This illustrates that it is not the height of injection nor the position of the top vent alone which matter but the distance separating the top vent from the injection.

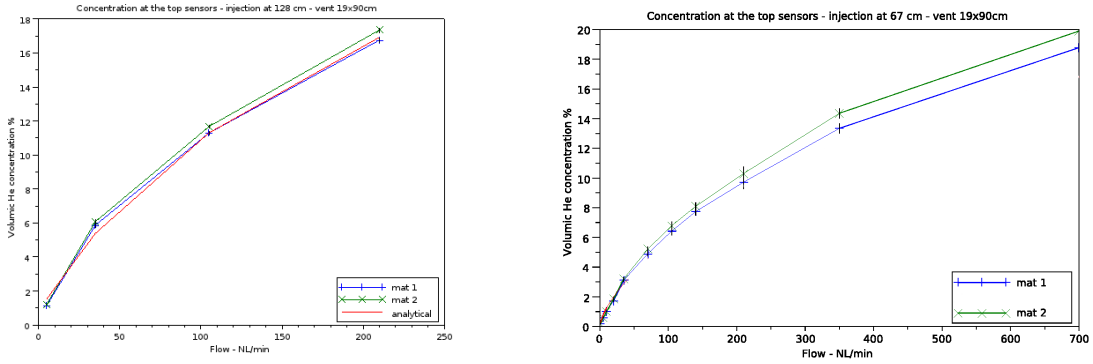

FIG. 9: Left: experimental concentration profile for an injection at 67 cm and the top vent located at 145 cm (mat 1 and 2) and analytical concentration profile for an injection at 128 cm and a top vent located at 206 cm. Altitude of the plotted results is shifted for the experimental curves so that both injections are superposed in order to compare the profiles. Right: experimental profile for an injection located at 67 cm and a top vent at 206cm hight.

D. Thickness layer quasi independant on the flow rate

Figure 10 presents, for a bi-layer regime, the thickness of the homogeneous upper layer according to the injection flow rate for an injection height of 27 cm. The tickness T is defined as an integral:

$$\int_0^H X_f(z)dz = Tmax(X_f(z)) \tag{5}$$

Therefore, the upper layer thickness is defined even when the layers are partially or totally stratified.

We observe that the thickness is almost independant of the flow rate, as predicted by the Linden model. Nevertheless, it has to be noticed a tendency to have a thicker layer at the lower flow rates when stratification starts to occur. In this situation, we are not in agreement with Linden hypothesis and furthermore the notion of layer thickness is not really significant.

E. Influence of the injection height versus top vent position

In this section experimental results obtained on helium build-up inside the 2 $\mathbf{m}^3$ enclosure according to the height of the injection are presented, for **the same top vent position**. Figure 11 shows for a release flow rate of 210 NL.min^{-1} the influence of the height of the injection on the maximal helium concentration measured inside the enclosure.

The maximal concentration of helium significantly increases with the height of injection. This experimental information highlights the importance of considering release height when known. **When using a simple model like Linden approach for example for risk assessment, we recommand that the height of the enclosure used in the model should be replaced in**

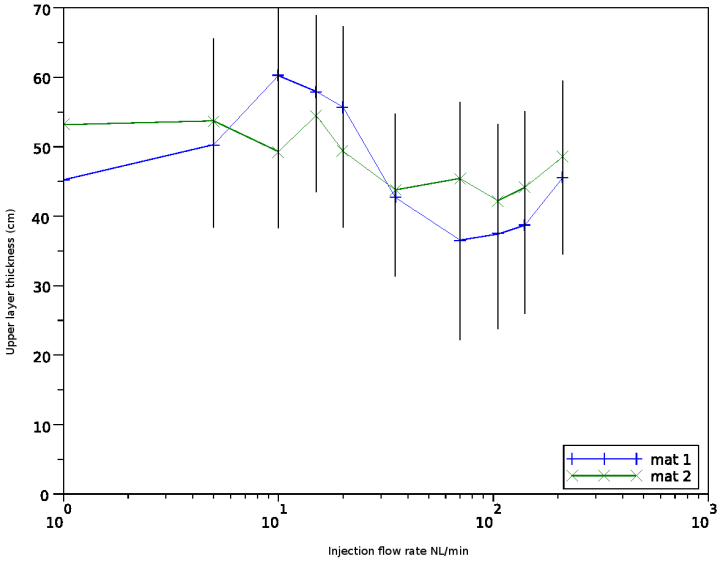

FIG. 10: Thickness of the upper homogeneous layer as a function of the injection flow rate at steady state for an injection height of 27 cm (vertical solid line: standard deviation), with one upper vent of h19 x w90 cm and one bottom vent of h19 x w90 cm.

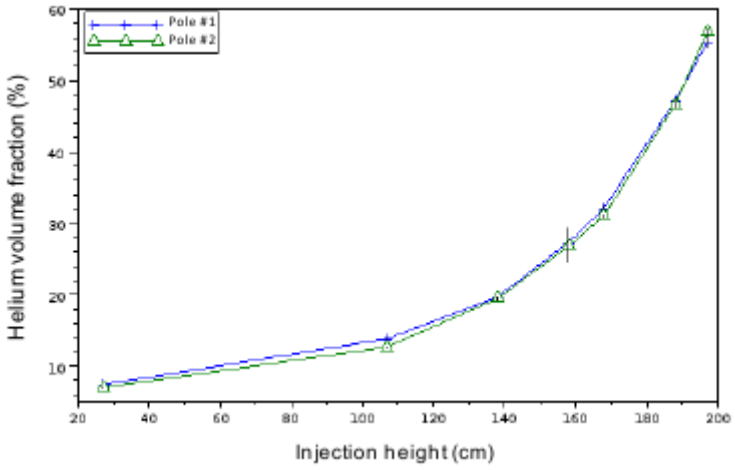

FIG. 11: Steady state maximal helium volume fraction as a function of the injection altitude for a 210 NL.min^{-1} release with two vents of 19 x 90 cm each (vertical solid line: standard deviation).

fact by the separating distance between the injection and the top vent (top edge of the top vent). In this case, the Linden model will give a better estimate of the concentration.

F. Inlfuence of injection-upper vent distance on the upper layer thickness

Since the upper layer thickness is more or less independant on the flow rate. We average the measured thickness obtained with all the flow rate for each configuration (ie distance injection - upper layer). We plot, Figure 12, the evolution of the upper layer thickness versus the separating distance between the injection and the upper vent.

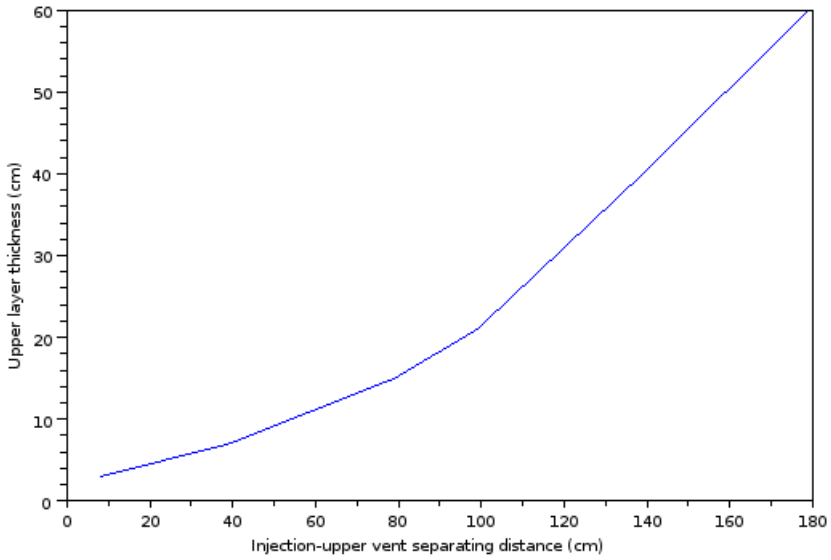

FIG. 12: Evolution of the upper layer thickness versus the injection-upper vent separating distance.

The thickness of the upper layer strongly increase with with increasing distance between the injection and the upper vent.

V. MODEL IMPROVEMENTS

A. Model construction

The model is relying on Linden hypothesis: the concentration distribution outside of the jet is 1-D along the vertical axis; there are two homogeneous layers; the volume concentration of helium in the upper layer is the concentration in the jet when entering the upper layer.

The improvement of the model [7] are the following: we solve the transient 1D conservation equations for the jet; we model the evolution of the entrainment coefficient alond the vertical axis; at last we solve the Bernouli equations at the vertical vent to correctly take into account the pressure variation at the vent.

As Linden [7] we define the neutral plan located at the height z_n such as:

$$P_i(z_n) = P_e(z_n), \tag{6}$$

where P_i is the pressure in the cavity and P_e the pressure outside the cavity. Above the pressure plan, the pressure inside the cavity is higher than outside and the flow at the vent is exiting the cavity. below the neutral plan, it is the opposite and the flow is entering the cavity. The second important parameter is the height of the interface separating the 2 homogeneous layers z_i. Below the interface, helium concentration is 0. Above the interface, the concentration is uniform.

The model consists in solving the following conservation equations:

$$Q_i + Q_{vi} = Q_{vo}, \tag{7}$$

where Q_i is the helium volumic flow rate at the injection, Q_{vi} is the mixture volumetric flow rate entering from outside at the vents surfaces located below z_n and Q_{vo} is the mixture volumetric flow rate exiting the cavity at the vents surfaces located above z_n. The Linden model assumes that the volumetric flow rate exiting the cavity is the same as the volumetric flowrate from the jet feeding the top layer at the interface:

$$Q_{vo} = Q_j(z_i), \tag{8}$$

where $Q_j(z_i)$ is the volumic flow rate if the mixture in the jet at the interface altitude. The mass conservation equation in the jet volume located in the lower layer (below z_i) is the following:

$$Q_j = \frac{g'_0}{g'} Q_0, \tag{9}$$

where the reduced gravity g':

$$g' = \frac{\rho_a - \rho}{\rho_a} g, \tag{10}$$

where ρ is the density of the mixture, ρ_a the density of air and g the gravity constant.

In order to close the system of unknowns, we have to model the behaviour in the jet, that is Q_j. Following works from Kaminski *et al* . [2], we introduce the following quatities for a free jet in an infinite media:

$$M(z) = \int_0^\infty r w^2(z, r) dr, \tag{11}$$

$$F(z) = \int_0^\infty r w g'(z, r) dr, \tag{12}$$

where z is the altitude, r the radial position around the jet axis and w the vertical velocity. We can derive from those integrals the axial velocity U, the volumetric flow rate Q and the top hat radius of the jet R, below the top layer:

$$U = \frac{F}{dM/dz} \tag{13}$$

$$Q = \frac{M}{U} \tag{14}$$

$$R = \sqrt{Q^2/M} \tag{15}$$

Under the Linden hypothesis (lower layer with pure air), we have the following conservation equations in the jet:

$$\frac{dQ}{dz} = 2\alpha M^{1/2}, \tag{16}$$

$$\frac{M}{dz} = \frac{FQ}{M}, \tag{17}$$

$$\frac{dF}{dz} = 0 \tag{18}$$

where α is the entrainment coefficient [2] defined as:

$$\alpha = \frac{C}{2} + (1 - \frac{1}{A})\frac{RF}{QU^2} + \frac{R}{2}\frac{d\ln A}{dz}, \tag{19}$$

where A is defined as:

$$A(z) = Aj, \qquad z < L_m \tag{20}$$

$$A(z) = A_j + \frac{1}{4}(A_p - A_j)(\frac{z}{L_m} - 1), \qquad L_m < z < 5L_m, \tag{21}$$

$$A(z) = A_p, \qquad z > 5L_m, \tag{22}$$

Where A_j and A_p are determined by kaminski [2] with a data fitting on a large database for pure jets or pure plumes behavior. Nevertheless we have modified their expression of those coefficients for the distances to the injection below 10 intection nozzle's diameters. Indeed, we dispose of a large database for lower distances. We finally use the following expressions for A_j and A_p:

$$A_j = 2.45 - (1.05 \exp(-0.004 * z/D)), \tag{23}$$

$$A_p = 0.64(1 + \text{thanh}(-0.1(\frac{z}{D} - 9))) + 0.825(1 + \text{thanh}(0.1(\frac{z}{D} - 7))), \tag{24}$$

where D is the diameter of injection. After an elimination process, we end up with a vectorial equation:

$$\frac{d}{dz}(M, Q) = (F_0 Q/M, 2\alpha M^{1/2}), \tag{25}$$

Which is a function of M and Q. A Runge Kutta method can be used to solve this system.

The final equation needed to close the system is using the charge loss coefficient $C_D = 0.6$ at the vents. The horizontal velocity V at the vents is connected to the pressure loss:

$$V^2 = 2C_D^2 \frac{\rho_a}{\rho_i} g'(z - z_n), \tag{26}$$

this velocity is connected to the volumic flow rates at the vents by integration, and according to the three possible scenarii concerning the interface and neutral plan positions.

The pressure profile is calculated in 3 configurations: both the interface and the neutral plan are above the bottom of the top vent, the neutral plane is above the bottom of the top vent and the interface is below, and finally both the interface and the neutral plan are located below the bottom of the top vent. It can be proved that the neutral plan is always located above the interface. The pressure profile is following a $\rho g z$ expression, ρ being the density of air outside of the box and below the interface according to Linden's model. ρ is the constant density of the mixture above the interface.

The system can be closed and lead to a non linear system to solve. The non linearity comes from the fact we have expressions changing according the three different scenarii for the interface and neutral plan positions. It is solved with an iterative algorithm.

B. Experimental results versus Linden model

In this section comparisons are performed between experimental data and theoretical predictions for build-up assessment in case of buoyant gas release in a naturally two-openings naturally ventilated volume. Figure 13 presents theoretical predictions of the helium maximal concentrations calculated with the Linden et al. methodology [7] as presented in the second section of the article. We illustrate the comparisons with the experimental data obtained for a 27 cm injection point. The injection flow rates vary from 1 to 210Â NL.min^{-1} . The Linden model was used with an entrainment coefficient of 0.1 and a discharge coefficient of 0.5 for the two openings. For release flow rates higher than 20Â NL.min^{-1} , the predicted values are significantly lower than the experimental data.

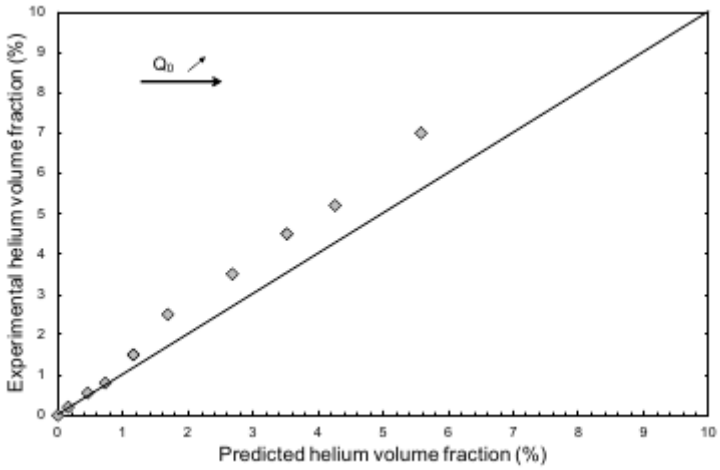

FIG. 13: Comparison of the experimental maximal helium volume fraction obtained for an injection height of 27 cm and the predicted values calculated from the Linden approach for a release at the floor at steady state, with two vents of h19 x w98 cm each.

C. Modified Linden model versus experiments

Figures 14 give comparisons on the maximal helium concentration between experiments (blue and green curves) and the fitted analytical approach developed through this work (red curves), for three different injection heights: (A) for a 27cm injection height, (B) for a 107 cm height injection and (C) for a 168 cm height injection.

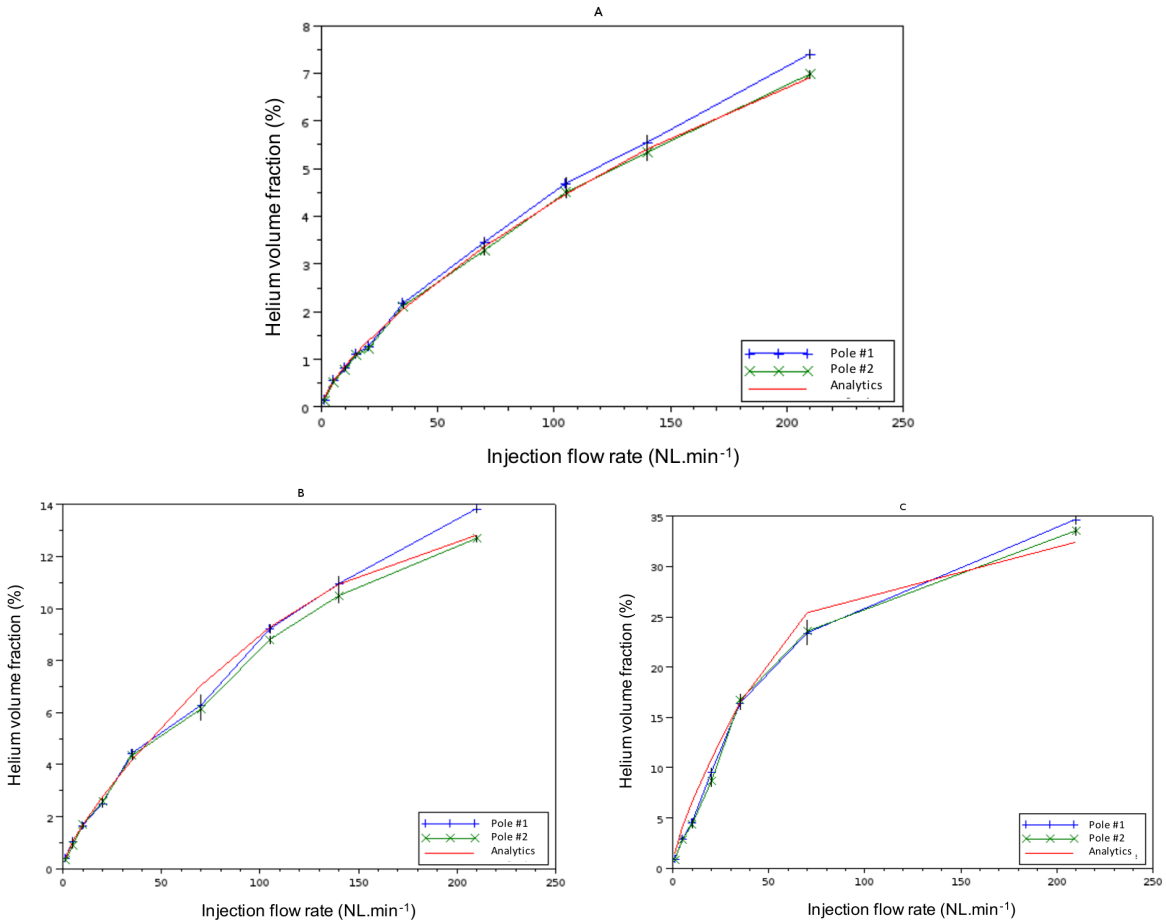

FIG. 14: Steady state maximal helium volume fraction as a function of the injection flow rate for several altitudes of release: 27 cm (A), 107 cm (B) and 168 cm (C) from the bottom, with two vents of h19 x w98 cm each.

These preliminary results are very satisfying since a good agreement is obtained whatever the release flow rate and whatever the injection point's height. However we observe that the model's behavior is degraded for the highest flow rate at 168 cm. This is explained by the fact that the bi-layer structure on which is based the model tends to disappear for an injection located above 168 cm as described Figure 8. The layer thickness is also well predicted by the model as shown Figure 15.

We notice that the models gives an almost constant thickness whatever the flow rate is. It was the case in Linden model, and the modifications concerning the vertical vents and the entrainment coefficient don't change that result. The experimental values show a larger thickness of the upper

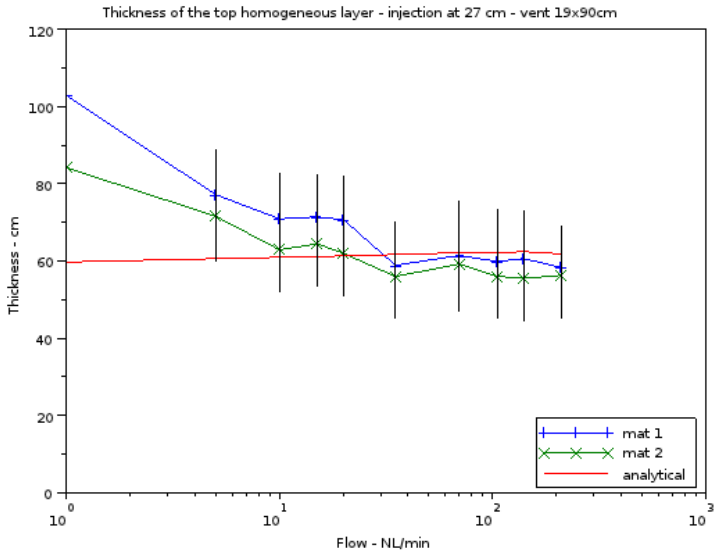

FIG. 15: Thickness of the upper layer for different flow rates and an injection located at 27 above the bottom of the enclosure.

layer for the lowest flow rates. This is due to the existence of a stratification for injected flow rates below 10 NL.min^{-1} . The model still manage to predict correct maximum concentration, but the thickness of the layer becomes miningless since no bi layer structure exist.

D. Limits of the approach

The main limit of the approach is when we are outside of the model hypothesis, that is when we have impining jets close to the ceiling of the enclosure, as shown Figure 8. A second limit is our choice for the coefficient A_j and A_p verified on our database, but which should be more extensively tested.

The next and final section's purpose is to understand how this bi-layer structure developp on a majority of cases and to find creteria to predict when the Linden model will apply.

VI. FLOW STRUCTURE IN A 2 VENTED CAVITY

This section has to be seen as a preliminary work on the subject. Results are promising but established on the smallest enclosure described in section 3. As we will see, the Linden bi-layer structure is not fully developped. Nevertheless it is the first step to validate both a numerical and an experimental process to obtain accurate velocity fields of the flow in a 2 vented cavity.

A. PIV measurement and numerical simulations

We present comparisons between the PIV experiments and Large Eddy Simulations performed by Saikali [5]. Comparisons are made on the time averaged quantities. The absolute statistical error is less than 0.02 m/s, having 400 uncorrelated velocity fields both with the fast and the PIV camera and around 800 for the numerical simulations. Turbulent fluctuations correlation time is less than 0.1s (around 0.05s). This is well described in [5].

We first represent the horizontal velocity profile at the bottom vent, Figure 16.

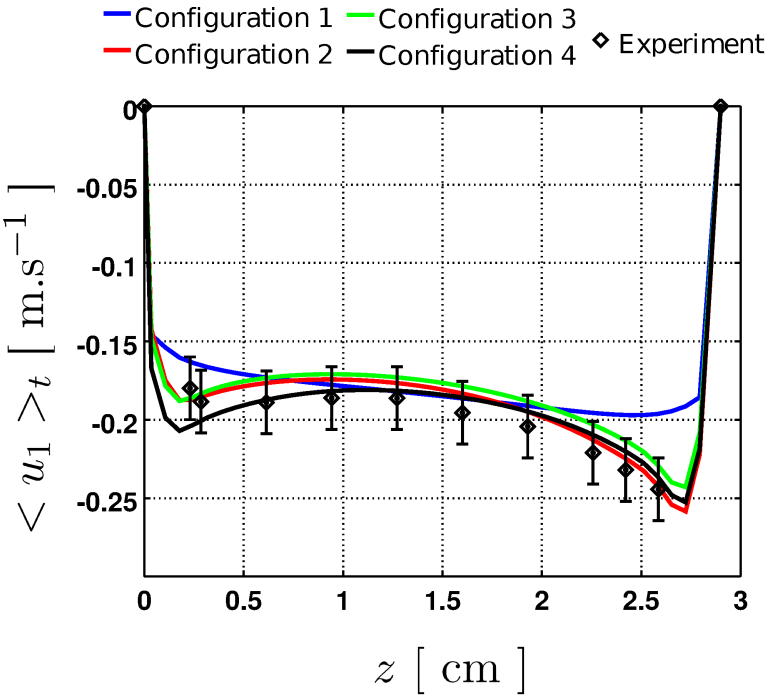

FIG. 16: Time averaged horizontal velocity profile at along the bottom vent in the laser $x0z$ plan. Configuration 1 to 4 correspond to L.E.S calculations. Experimental results are those obtained with the fast camera and a 1 every 5 pictures correlation procedure.

The configuration 1 correspond to a numerical simulation performed without an outer domain and boundary conditions directly applied to the vents. Configuration 2 to 4 correspond to simulations performed with an outer domain, on wich are applied the boundary conditions. Configuration 4 has le larger outer domain, and is therefore closer to the reality. Comparisons show a very good agreement between experimental measurements and configuration 4 results.

We also perform a comparison of the same profiles for the 2 experimental types of acquisition: the fast camera and the PIV camera, Figure 17. The acquisitions are achieved on two separated times: a first experiment with the fast camera, then a change of camera and another run of measurements. This also contributes to check the reproducibility of the results. We notice that the results are within the statistical and measurements errors. The main differences are located near the top and bottom sides of the vent. Indeed, PIV measurements are achieved with a more powerfull laser which creates stronger light reflexions on surface edges. Measurements are therefore erroneous very near the sides (velocities are slower than reality).

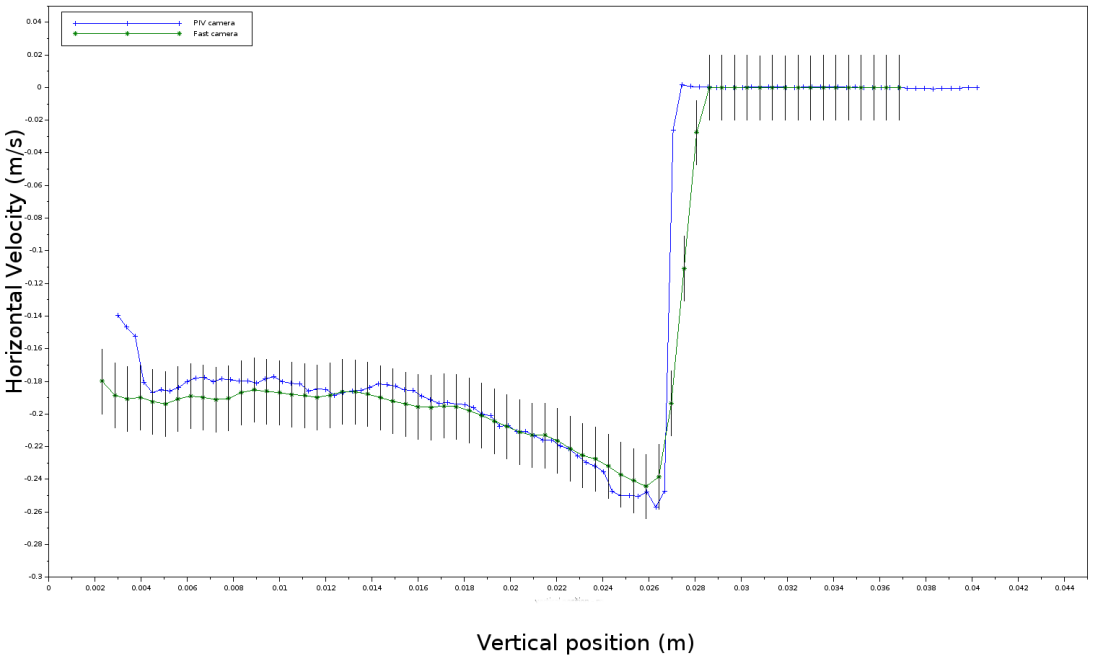

FIG. 17: Time averaged horizontal velocity profile at along the bottom vent in the laser $x0z$ plan. Comparison between two acquisition methods: with a PIV camera and with a fast camera.

We show the obtained time averaged velocity norm $\sqrt{u_x^2 + u_z^2}$, for the experiment and for the numerical simulations, Figure 18.

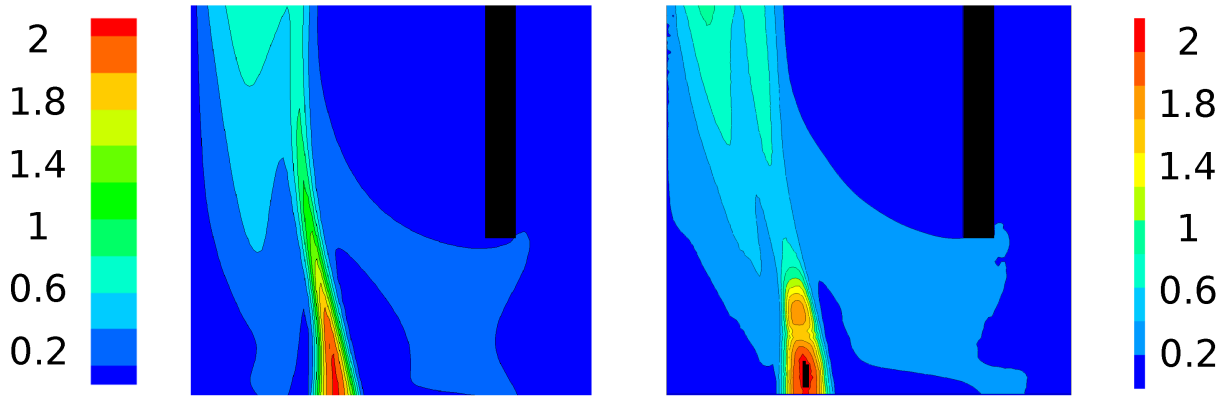

FIG. 18: Time averaged velocity norm. L.E.S calculations left, experiments right.

Again, results show strong similarities: same velocities intensity, same inclination of the jet and apparition of a second structure at the left of the jet. We also observe a laminar to turbulent transition occuring between 3 to 6 cm above the bottom of the cavity, Figure 19.

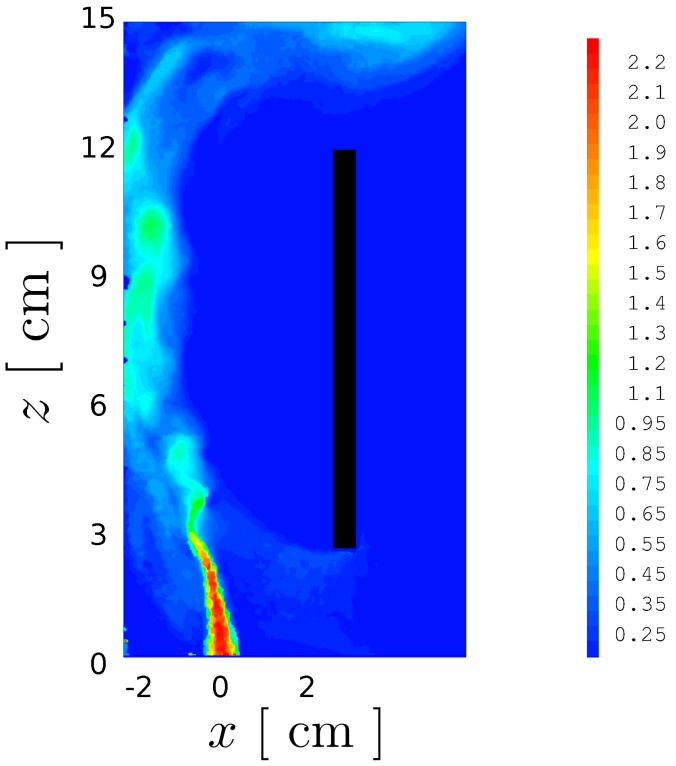

FIG. 19: Instantaneous velocity norm. Experiments with PIV camera.

B. Helium Concentration distribution

The interest of the numerical results lies in their availability in the complete domain, instead of just in a 2D plan. The second interest is that we have access to the volumic concentration distribution. We can't perform those measurements in the small cavity due to the size of the concentration sensors (too intrusive at that scale). CFD simulations being validated with grid convergence [5] and also against our experiments, we now are entitled to fully use numerical results to better understand the flow structure in the cavity.

As we have illustrated in the previous section, a two layer structure appears in most of the situations for a two vented cavited. We plot, Figure 20, some helium volumic concentration's vertical profiles, at different locations of the enclosure.

We can see that for the curves A, H and B - which corresponds to sensors located alond the vented wall - a change of concentration similar to Linden prediction occurs around $z = 9cm$. For the curves C, G , F, D we notice a smoother change of concentration with a plateau reached around $z = 12cm$. At last, for the E curve, the plateau is reached smoothly around $z = 6cm$, where the steady concentration is the same as along the jet axis. The averaged profile on the right figure shows that we don't reproduce the Linden behaviour, which is explained by the non uniform horizontal distribution of helium due to the strong interaction with the left wall (facing the vents). In fact, the enclosure is not large enough to be in a situation where Linden model applies.

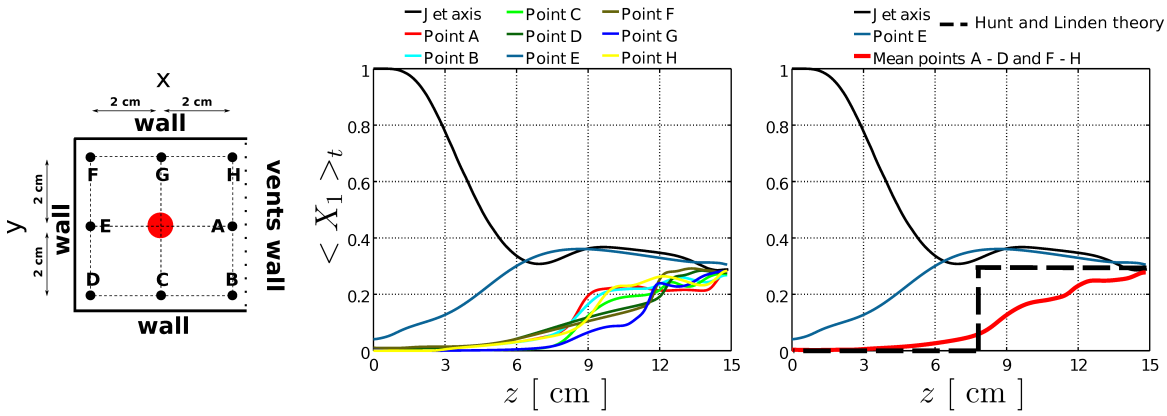

FIG. 20: Helium volumic concentration's vertical profiles. CFD results.

Nevetheless, this preliminary set up is interesting since it gives explanation to the flow structure and the concentration distribution, which will be extended in a following work with a larger enclosure. At first, Figure 21, we observe two eddies in the x0z plan, formed by the interaction of the jet with the ceiling of the box and the two lateral vertical walls. Those eddies are approximately 3 cm wide, and that explains the plateau reached by the curves C, G, D and D, directly influenced by those structures.

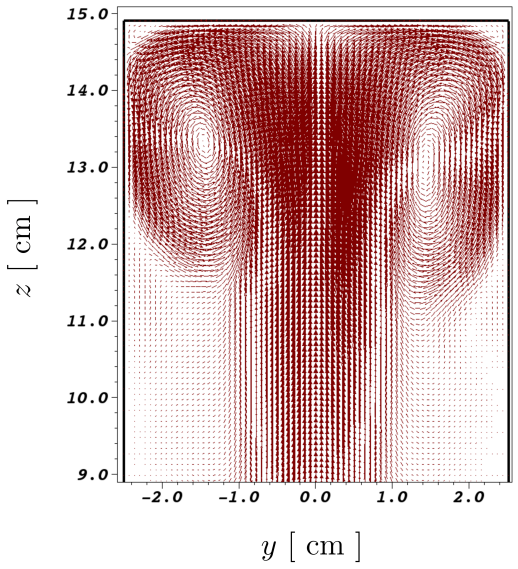

FIG. 21: Time averaged velocity field in x0z plan at the top of the enclosure. CFD calculation.

Then, Figure 21, we observe strong interaction between the jet and the back wall - facing the vents. That explains why the concentration in the E curve and in the jet are almost similar above 6 cm high.

If we zoom near the top vent in the picture 22, see Fig. 23, we observe an eddy structure down to approximately $z = 9cm$. This explains why a plateau is reached at that altitude for the curves A, H and B.

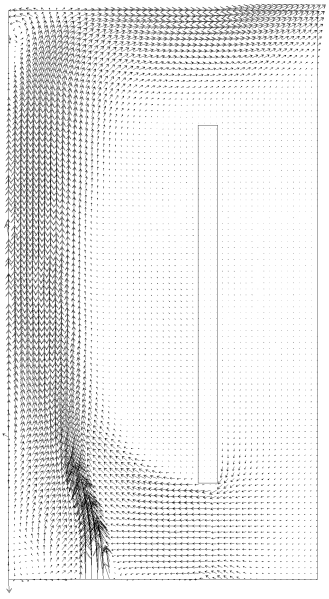

FIG. 22: Time averaged velocity field in y0z plan. PIV measurements.

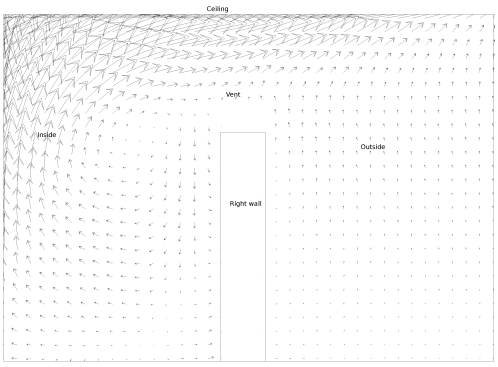

FIG. 23: Time averaged velocity field in y0z plan. PIV measurements.

As a conclusion, we observe that Linden prediction is located in between our different mat curves. The plateau concentration predicted by Linden is in good aggreement with the observed concentration at the top of the enclosure. All the observed volumic concentrations converge to an almost similar value around 30% at the top.

Now that we are able to obtain consistent results between experiments and CFD calculations, we are going to study a wider set-up, where jet-walls interactions are reduced in order to observe clearly the Linden two layers structure and validate criteria of existence or non existence of such a structure.

VII. DISCUSSIONS AND CONCLUDING REMARKS

Experiments on the dispersion of a helium release in a 2 $\mathbf{m}^3$ rectangle parallelepiped with a square horizontal base enclosure equipped with two openings for natural ventilation were performed to assess the effects of the injection flow rate and of the height of the release source on the helium volume fraction and on the distribution profile. Injection flow rates, corresponding to volume Richardson numbers higher than 1, cover the $[1 - 210]$ NL.min^{-1} range.

The study of the height of the injection point allowed the observation of several phenomena. The most important result is that **only the distance separating the injection from the top vent matters** at steady state. The location of the ceiling, above the top vent, has only a storage influence. The higher the ceiling, the longer it takes to fill the region above the top vent and therefore to reach a steady state. However the homogenous concentration of the top layer won't be affected. **It is therefore recommanded to use the separating height between the upper edge of the top vent and the injection in the Linden model as a replacement for the cavity's height**.

A large injection-top vent distance and a small injection's flow rate promote a stratification, a larger flow rate or a smaller separating distance promote a bi-layer regime. But when the the distance is too significantly decreased, the bi-layer structure disappears; a third regime is observed: an impinging regime without a homogeneous layer.

To complete this experimental work, two theoretical approaches were studied: first the Linden et al. methodology commonly used, and an improved model taking into account the vertical vents and a varying entrainment coefficient [2]. Results show that the Linden approach is not conservative for the helium maximal concentration assessment when the injection point is not at the bottom of the enclosure for flow rates higher than 20 NL.min^{-1} . More accurate results were obtained with a varying entrainment coefficient.

At last, PIV measurements and CFD calculations showed very good agreement on a smaller set-up. Access to the velicoty field gives a better understanding of the homogeneous laye's formation, as predicted by Linden. Further works have to be performed on a larger set-up in order to validate prediction criteria for the existence or non-existence of the Linden bi-layer structure.

VIII. ACKNOWLEDGMENTS

The results presented in this paper have been obtained within the frame of the Horizon Hydrogène Energie (H2E) program. The authors acknowledge the French agency for innovation support OSEO, and CEA for technical, experimental and scientific support.

[1] G. Bernard-Michel, *Rapport d'essais regroupant l'ensemble des résultats expérimentaux obtenus sur les rejets en milieu confiné (ec04)*, Rapport Technique (4.1).6.EC04, H2E (2012).

[2] E. Kaminski, G. Carazzo, and S. Tait, *On the rise of turbulent plumes: quantitative effects of variable entrainment for submarine hydrothermal vents, terestrial and extra terrestrial explosive volcanism*, Journal of geophysical research **113** (2008).
[3] B. Cariteau, Rapport DM2S/SFME/LEEF RT/2012-016/A, CEA (2012).
[4] G. R. Hunt and P. F. Linden, *Displacement and mixing ventilation driven by opposing wind and buoyancy*, J. Fluid Mech. **527**, 27 (2005).
[5] E. Saikali, G. Bernard-Michel, A. Sergent, C. Tenaud, and R. Salem, *Reference large eddy simulations of a laminar-turbulent transitional air-helium buoyant jet in a two vented enclosure: validation against particle image velocimetry experiments*, ICHS (2017).
[6] B.-M. G. and H. D., *Comparison of helium and hydrogen releases in 1 m3 and 2 m3 two vents enclosures: Concentration measurements at different flow rates and for two diameters of injection nozzle*, Int. J. Hydrogen Energy **42**, 7542 (2017).
[7] P. F. Linden, *The fluid mechanics of natural ventilation*, Annual Review Fluid Mechanics **31**, 201 (1999).
[8] P. F. Linden, G. F. Lane-Serff, and D. A. Smeed, *Emptying filling boxes : the fluid mechanics of natural ventilation*, J. Fluid Mech. **212**, 309 (1990).
[9] W. D. Baines and J. S. Turner, *Turbulent buoyant convection from a source in a confined region*, J. Fluid Mech. **37**, 51 (1967).
[10] G. I. Taylor, B. R. Morton, and J. S. Turner, *Turbulent gravitational convection from maintained and instantaneous source*, Proc. R. Soc. Lond. **234**, 1 (1996).
[11] C. J. Chen and W. Rodi, *Vertical turbulent buoyant jets: a review of experimental data*, Nasa STI/Recon Technical Report A **80** (1980).